ELSEVIER

Chemical Engineering Science 60 (2005) 5991–6003

Chemical Engineering Science

www.elsevier.com/locate/ces

Global modelling of a gas–liquid–solid airlift reactor

Samuel Talvy*, Arnaud Cockx, Alain Line

Laboratoire d'Ingénierie des Procédés de l'Environnement, D.G.P.E., I.N.S.A., 135, Avenue de Rangueil, 31077 Toulouse cedex 04, France

Received 17 November 2004; received in revised form 20 April 2005; accepted 20 April 2005
Available online 6 July 2005

Abstract

This paper presents a global model of three phase flow (gas–liquid–solid) in an internal airlift reactor. The airlift is composed of four zones: a riser (on the aerated side on the internal wall), a downcomer (on the opposite side) and two turning zones above and below the internal wall. Tap water is the liquid continuous phase and the dispersed phases are air bubbles and polyethylene particles. The global modelling of the airlift involves mass and momentum equations for the three phases. The model enables phase velocities and phase volume fractions to be estimated, which can be compared to experimental data. Closure relations for the gas and solid drift velocities are based on the model proposed by Zuber and Findlay. The drift flux coefficients are derived from CFD numerical simulations of the airlift. Gas bubble and solid particle averaged slip velocities are deduced from momentum balances, including drag coefficient correlations. The link between Zuber and Findlay model and the two-fluid model is established. In the experiment as well as in the model, the gas flow rate is fixed. However, the liquid and solid flow rates are unknown. Two closure relations are needed to predict these flow rates: the first closure relation expresses that the volume of solid injected into the airlift remains constant; the second closure relation expresses a global balance between the difference of column height in the riser and the downcomer and the total pressure drop in the airlift. The main parameters of a three phase airlift reactor, like gas and solid volume fractions, are well predicted by the global model. With increasing solid filling rate (40%), the model starts to depart from the experimental values as soon as coalescence of bubbles appears.

Keywords: Gas–liquid–solid; Airlift reactor; Hydrodynamics; Modelling

1. Introduction

Airlift reactors are mainly used in biological processes and can also be helpful for waste water treatment. In this case, nitrification can be achieved by biomass growing on fluidized particles in a gas–liquid–solid airlift reactor. The air flow in the airlift oxygenates the biomass and induces a global circulation of solid particles. The main value of an airlift reactor (ALR) is the presence of a permanent liquid circulation which induces a rather low shear stress on the particles where biofilm grows (Heijnen et al., 1992). Two types of vessels can be found in the literature (Siegel and Robinson, 1992): internal loop airlifts (IL-ALR) and external loop airlifts (EL-ALR). IL-ALR is a rectangular or cylindrical vessel separated on the inside with a baffle in order to establish liquid circulation. EL-ALR is composed of separate vessels for the aerated zone and the non-aerated zone which are linked by pipes and permits the liquid circulation.

IL-ALR and EL-ALR have been widely studied experimentally. These studies mainly focus on liquid velocity circulation, gas and solid phase hold-ups (van Benthum et al., 2000) and on mass transfer (Nicollela et al., 1999). Merchuk (2003) drew up a review of previous works published about the airlift loop reactors. Among all the former works concerning airlift modelling, few of the them (Cockx et al., 1997; Oey et al., 2001) dealt with the computational fluid dynamics (CFD) approach for two phase flow. Many global models have also been developed by various authors for two-phase flow: Heijnen et al. (1997), Saez et al. (1998), Freitas et al. (1999) and Couvert (2000).

* Corresponding author. Tel.: +33 56155 9798; fax: +33 6155 9760.
E-mail addresses: talvy@insa-toulouse.fr (S. Talvy), alain.line@insa-toulouse.fr (A. Line).

0009-2509/$ - see front matter © 2005 Elsevier Ltd. All rights reserved.
doi:10.1016/j.ces.2005.04.067

This study continues on from the previous works accomplished by Cockx et al. (1997), Cockx (1998) and Couvert (2000) but with three phases. The objective is to perform a simple global model to describe the hydrodynamics for a gas–liquid–solid IL-ALR. Therefore, to reach this objective, the global model equations are first presented and simplified. Afterwards, closure relations are also detailed, the experimental setup is described and results are presented for two different solid loadings. The interesting aspect of this work is to implement data from three phase CFD simulations which provide different unknown terms necessary to close the global model equations.

2. Global model of gas–liquid–solid flow

The mass and momentum equations are written in the continuous liquid phase and in the two dispersed phases (gas bubbles and solid particles). The local equations are firstly recalled. Space averaging of both variables and equations enable the model to be simplified.

2.1. Local Navier–Stokes equations in multiphase flow

The following equations express mass (Eq. (1)) and momentum (Eq. (2)) balances in multiphase flow and in Eulerian–Eulerian framework. The subscript k stands for each phase.

$$\frac{\partial(\alpha_k\rho_k)}{\partial t} + \nabla(\alpha_k\rho_k u_k) = \dot{m}_k. \tag{1}$$

Where ρ_k and α_k represent, respectively, the density and volume fraction of phase k. On the right hand side, $\dot{m}_k$ represents mass transfer at the interface between the phase k and the two other phases. For the sake of simplicity, interfacial mass transfer is not considered in the present work. $\dot{m}_k$ is thus equal to zero.

$$\frac{\partial(\alpha_k\rho_k u_k)}{\partial t} + \nabla(\alpha_k\rho_k u_k u_k) = -\alpha_k\nabla P_k + \alpha_k\nabla(\tau_k - \rho_k\overline{u'_k u'_k}) + \alpha_k\rho_k g + M_k, \tag{2}$$

where u_k represents the velocity of phase k. On the right hand side, P is the pressure, τ_k is the viscous stress tensor and $\rho_k\overline{u'_k u'_k}$ is the turbulent Reynolds stress tensor. g is the gravitational acceleration. M_k represents the transfer of momentum at the interface between phase k and the two other phases. This term is essential in multiphase flow dynamics since it accounts for drag between dispersed and continuous phases, for example. This term accounts for drag, added mass and turbulent pressure. It can be expressed in bubbly two-phase flow as (Mudde and Simonin, 1999)

$$\overline{M_G} = -\overline{M_L} = a\tfrac{1}{2}\rho_L C_D \overline{u_r}\,\overline{v_r} + \alpha_G\rho_L C_A\left[\frac{\partial\overline{u_r}}{\partial t} + \overline{u_G}.\nabla\overline{u_r}\right] + \nabla[\alpha_G\rho_L C_A\overline{u'_G u'_r}] - \rho_L\overline{u'_G u'_L}.\nabla\alpha_G,$$

where u_r is the relative velocity

$$\overline{u_r} = \overline{u_G} - \overline{u_L},$$

v_r will be defined later, C_A is the added mass coefficient, C_D is the drag coefficient and a is the interfacial projected area.

The first term on the right hand side of the previous equation accounts for drag. It will only be discussed below, since the circulation in the airlift is controlled by the gas flow, and primarily by buoyancy effects. In the momentum equation of the two-fluid model, the interfacial transfer of momentum related to drag is expressed as

$$\overline{M_G} = -\overline{M_L} = a\tfrac{1}{2}\rho_L C_D\overline{u_r}\,\overline{v_r}.$$

The relative velocity v_r is not equal to the difference of velocity of the two phases. It is defined as

$$\overline{v_r} = \overline{u_G} - \overline{u_L} - \overline{v_{dr}}.$$

The relative velocity $\overline{v_r}$ is the statistical average of the local instantaneous relative velocity between each bubble and the surrounding liquid. In other words, it represents the statistical average of relative velocity of the liquid seen by the gas. The statistical average of the turbulent fluctuating liquid velocity in the liquid is equal to zero but the statistical average of the turbulent fluctuating liquid velocity seen by the gas is not equal to zero. It is written $\overline{v_{dr}}$, in terms of local drift velocity (Simonin and Viollet, 1990). Formally, the drift velocity $\overline{v_{dr}}$ is modelled as

$$\overline{v_{dr}} = -D_{\text{local}}\frac{1}{\alpha_g}\nabla\alpha_g, \tag{3}$$

where D_{local} is a local diffusivity accounting for turbulent dispersion of gas bubble and $\nabla\alpha_g$ is the spatial gradient of the gas fraction. This term $\overline{v_{dr}}$ plays a key role in the local modelling of dispersion of gas in bubble columns (Mudde and Simonin, 1999) and airlift reactors (Talvy, 2003).

In the present work, these local equations will not be solved. In a first approach, a more global model is developed after space averaging of these equations. In the closure problem of the global model, CFD results developed by Talvy (2003) and based on the numerical solution of these local equations will be used.

2.2. Global model of gas–liquid–solid reactor in steady state and fully developed flow

The objective of the global model is to provide averaged values of gas, liquid and solid velocities and volume frac-

tions in order to globally characterize the hydrodynamics of the gas–liquid–solid airlift reactor.

The spatial average of volume fraction of the phase k denoted by R_k is defined by

$$R_k = \langle \alpha_k \rangle = \frac{1}{A} \int \int_A .\alpha_k \, \mathrm{d}s, \tag{4a}$$

where $\langle\rangle$ stands for the spatial averaging operator. A is the cross sectional area of the flow. Given a variable f_k, one can derive

$$R_k \langle \langle F_k \rangle \rangle = \langle \alpha_k f_k \rangle = \frac{1}{A} \int_A .\alpha_k \int f_k \, \mathrm{d}s. \tag{4b}$$

For the sake of simplicity, once the spatial averaging operator is applied to the equations, the averaged value $\langle\langle F_k \rangle\rangle$ will be simply written as F_k.

Mass balance equation:

Space averaging of Eq. (1) can be derived and simplified in the case of a steady state and fully developed flow. In addition, the section A is assumed to be constant, interfacial mass transfer is neglected and the walls of the reactor are assumed to be impermeable. It becomes

$$R_k U_k = cons \tan t.$$

One can define the superficial velocity of phase k, represented by j_k, as the volumetric flow rate of phase k, noted as Q_k, divided by the section A.

$$R_k U_k = \frac{Q_k}{A} = j_k. \tag{5}$$

In other words, the flow rate of phase k is equal to the product of the velocity and the cross sectional area occupied by phase k, denoted by A_k

$$Q_k = A_k U_k = A j_k.$$

Indeed, the mass balance expresses that the velocity of phase k will adapt to the section occupied by phase k in order to conserve the flow rate. The momentum equation is needed to determine the volume fraction and the phase velocity.

Momentum balance equation:

Following the same derivation, Eq. (2) becomes

$$R_k \frac{\partial P}{\partial z} = \frac{1}{A} L_k^w \tau_k^w + \sum_{\substack{k,l=1 \\ k \neq l}}^{3} a_{k,l}^i \tau_{k,l}^i - R_k \rho_k g, \tag{6}$$

L_k^w represents the perimeter of the wall wetted by phase k and τ_k^w stands for the wall shear stress exerted by phase k. $a_{k,l}^i$ represents the projected interfacial area between phase k and phase l per unit volume. $\tau_{k,l}^i$ stands for the stress exerted by phase k on phase l, resulting from pressure and viscous stress distribution along the interface. In steady state and fully developed flow, it reduces to drag.

In multiphase flow, the sum of the different phase volume fractions is equal to unity.

$$\sum_{k=1}^{3} R_k = 1. \tag{7}$$

These mass (Eq. (5)) and momentum (Eq. (6)) equations (detailed for the gas, liquid and solid phases) and the geometrical relation (Eq. (7)) involve a system of seven equations with seven variables: the three volume fractions (R_g, R_l, R_s), the three velocities (U_g, U_l, U_s) and the pressure gradient ($\mathrm{d}P/\mathrm{d}z$). In the system, additional variables appear: the gas, liquid and solid superficial velocities (respectively, j_g, j_l and j_s), the wall perimeters wetted by the phases (L_k^w), the associated wall shear stresses (τ_k^w), the interfacial areas ($a_{k,l}^i$) and the associated stress ($\tau_{k,l}^i$). As will be detailed in the next section, most of these additional variables need closure relations.

2.3. Decoupling of the pressure gradient derivation

Generally, the three momentum equations, corresponding to each phase, are combined so as to obtain an equivalent set of equations in which the pressure gradient calculation is separated from the calculation of the other variables.

The three momentum equations are written below:

$$R_g \frac{\partial P}{\partial z} = \frac{1}{A} L_g^w \tau_g^w + a_{g,l}^i \tau_{g,l}^i + a_{g,s}^i \tau_{g,s}^i - R_g \rho_g g, \tag{8a}$$

$$R_l \frac{\partial P}{\partial z} = \frac{1}{A} L_l^w \tau_l^w + a_{l,g}^i \tau_{l,g}^i + a_{l,s}^i \tau_{l,s}^i - R_l \rho_l g, \tag{8b}$$

$$R_s \frac{\partial P}{\partial z} = \frac{1}{A} L_s^w \tau_s^w + a_{s,l}^i \tau_{s,l}^i + a_{s,g}^i \tau_{s,g}^i - R_s \rho_s g. \tag{8c}$$

To simplify these equations, assumptions have to be made. Since both gas and solid phases are dispersed, we can assume that there is no interfacial transfer between gas bubbles and solid particles. Thus

$$a_{g,s}^i \tau_{g,s}^i = -a_{s,g}^i \tau_{s,g}^i = 0.$$

The transfers between each dispersed phase and the continuous liquid phase verify the following equality:

$$a_{g,l}^i \tau_{g,l}^i = -a_{l,g}^i \tau_{l,g}^i \quad \text{and} \quad a_{s,l}^i \tau_{s,l}^i = -a_{l,s}^i \tau_{l,s}^i.$$

The transfer of momentum between each dispersed phase and the wall can be neglected. Thus:

$$L_g^w \tau_g^w = L_s^w \tau_s^w = 0.$$

It becomes

$$R_g \frac{\partial P}{\partial z} = a_{g,l}^i \tau_{g,l}^i - R_g \rho_g g, \tag{9a}$$

$$R_l \frac{\partial P}{\partial z} = \frac{1}{A} L_l^w \tau_l^w - a_{g,l}^i \tau_{g,l}^i - a_{s,l}^i \tau_{s,l}^i - R_l \rho_l g, \tag{9b}$$

$$R_s \frac{\partial P}{\partial z} = a^i_{s,l}\tau^i_{s,l} - R_s\rho_s g. \quad (9c)$$

The sum of these three equations gives mixture momentum, as follows:

$$\frac{\partial P}{\partial z} = -(R_g\rho_g + R_l\rho_l + R_s\rho_s)g + \frac{1}{A}L^w_l\tau^w_l. \quad (10)$$

Adding Eqs. (9b) and (9c) leads to the expression of the momentum of a pseudo-liquid–solid mixture:

$$\frac{\partial P}{\partial z} = -\frac{a^i_{g,l}\tau^i_{g,l}}{1-R_g} - \frac{R_l\rho_l + R_s\rho_s}{1-R_g}g + \frac{1}{A(1-R_g)}L^w_l\tau^w_l,$$

Eq. (9a) is equivalent to

$$\frac{\partial P}{\partial z} = \frac{a^i_{g,l}\tau^i_{g,l}}{R_g} - \rho_g g.$$

Equating the left hand side of the two previous gives

$$a^i_{g,l}\tau^i_{g,l} = R_g\left[(\rho_g - \rho_M)g + \frac{1}{A}L^w_l\tau^w_l\right]. \quad (11a)$$

The same derivation can be applied to Eqs. (9a) and (9b). It becomes

$$a^i_{s,l}\tau^i_{s,l} = R_s\left[(\rho_s - \rho_M)g + \frac{1}{A}L^w_l\tau^w_l\right]. \quad (11b)$$

The subscript M is assigned to the mixture:

$$\rho_M = \rho_l R_l + \rho_g R_g + \rho_s R_s.$$

Eqs. (10), (11a) and (11b) can been substituted to Eqs. (9a)–(9c). Thus, the derivation of the pressure gradient can be decoupled from the calculation of the six other variables. Finally, six equations are retained (Eq. (5)) for each phase, Eqs. (7), (11a) and (11b) to calculate the six unknown variables (R_g, R_l, R_s, U_g, U_l, U_s), providing the additional variables are known. Then, the pressure gradient is determined from Eq. (10).

2.4. GLS drift flux model

In Eqs. (11a) and (11b), the drag is mainly balanced by the gravity term, since the momentum transfer at the wall is at least one order of magnitude smaller than gravity. These equations can be used to estimate the averaged slip velocities of gas bubbles and solid particles. Neglecting wall momentum transfer, Eqs. (11a) and (11b) reduce to

$$a^i_{g,l}\tau^i_{g,l} = R_g(\rho_g - \rho_M)g$$

and

$$a^i_{s,l}\tau^i_{s,l} = R_s(\rho_s - \rho_M)g.$$

Modelling the interfacial momentum transfer in a classical way, the projected area $a^i_{g,l}$ is related to the gas bubble diameter d_g and to the gas fraction R_g as

$$a^i_{g,l} = \frac{3R_g}{2d_g},$$

the stress $\tau^i_{g,l}$ resulting from pressure and viscous stress distributions on the bubbles induces a drag term and can thus be closed in terms of liquid–solid mixture density, drag coefficient $C_{D,g}$ and slip velocity G as

$$\tau^i_{g,l} = -\frac{1}{2}\frac{\rho_s R_s + \rho_l R_l}{1-R_g}C_{D,g}G^2.$$

One can easily derive the following expression:

$$\frac{\rho_s R_s + \rho_l R_l}{1-R_g} = \frac{\rho_M - \rho_g R_g}{1-R_g}.$$

Thus, the slip velocities of the gas bubbles and solid particles can be calculated as

$$G = \sqrt{\frac{4}{3}g\frac{d_g}{C_{D,g}}\frac{(\rho_M - \rho_g)(1-R_g)}{\rho_M - \rho_g R_g}} \quad (12a)$$

for the bubble slip velocity, where $C_{D,g}$ is the drag coefficient for gas bubbles

$$S = \sqrt{\frac{4}{3}g\frac{d_s}{C_{D,s}}\frac{|\rho_M - \rho_s|(1-R_s)}{\rho_M - \rho_s R_s}}\frac{\rho_M - \rho_s}{|\rho_M - \rho_s|} \quad (12b)$$

for the solid slip velocity, where $C_{D,s}$ is the drag coefficient for solid particles. In other words, Eqs. (11a) and (11b) enables to express the global slip velocities G and S.

As mentioned in Section 2.1, in the local approach based on the two-fluid model, the relative velocity involved in the drag accounts for two terms, the relative mean velocity and an additional term called local drift velocity.

Therefore, the averaged slip velocities G and S can be written as

$$G = U_g - j_M - V_{dr,g},$$

$$S = U_s - j_M - V_{dr,s},$$

where $V_{dr,g}$ and $V_{dr,s}$ are the averaged drift velocities of gas bubbles and solid particles. In fact, the following expressions issued from Zuber and Findlay model enable to express the drift velocities of each phase:

$$G = U_g - C_{0,g}(j_g + j_l + j_s) = U_g - j_M - (C_{0,g} - 1)j_M,$$

$$S = U_s - C_{0,s}(j_g + j_l + j_s) = U_s - j_M - (C_{0,s} - 1)j_M,$$

hence

$$V_{dr,g} = (C_{0,g} - 1)j_M$$

and

$$V_{dr,s} = (C_{0,s} - 1)j_M.$$

In two-phase bubbly flow for example, the drift flux coefficient is defined as follows:

$$C_{0,g} = \frac{\langle\alpha_g j_M\rangle}{\langle\alpha_g\rangle\langle j_M\rangle} = 1 + \frac{\langle\alpha''_g j''_M\rangle}{\langle\alpha_g\rangle\langle j_M\rangle}.$$

The exponent $''$ expresses the local difference between the local value and the space averaged value of gas fraction and

Table 1
GLS model basic equations

$$R_g U_g = \frac{Q_g}{S} = j_g$$
$$R_l U_l = \frac{Q_l}{S} = j_l$$
$$R_S U_s = \frac{Q_s}{S} = j_s$$
$$R_g + R_l + R_S = 1$$
$$U_g = C_{0,g}(j_g + j_l + j_s) + G$$
$$U_s = C_{0,s}(j_g + j_l + j_s) + S$$

mixture velocity. $C_{0,k}$ is thus related to the non-uniformity of the multiphase flow field in the cross-section. $C_{0,k}$ will be determined by numerical simulations in the present work. In the future, the modelling of $C_{0,k}$ could be developed in terms of gradient assumption. In this scope, it would be possible to write formally:

$$\langle \alpha_g'' j_M'' \rangle = -D_{\text{global}} \langle \nabla \alpha_g \rangle.$$

Thus, the global drift velocity writes

$$V_{dr,g} = (C_{0,g} - 1) j_M = -D_{\text{global}} \frac{1}{\langle \alpha_g \rangle} \langle \nabla \alpha_g \rangle$$

which is consistent with the local modelling of drift velocity (see Section 2.1, Eq. (3)). In the global approach, the global diffusivity D_{global} accounts both for turbulent dispersion and spatial dispersion.

For sake of simplicity, in the following we will refer to the drift model of Zuber and Findlay (1965):

$$U_g = C_{0,g}(j_g + j_l + j_s) + G, \tag{13a}$$

$$U_s = C_{0,s}(j_g + j_l + j_s) + S, \tag{13b}$$

where $C_{0,k}$ is a modelling parameter, given by CFD in this work and where G and S are given by Eqs. (12a) and (12b), resulting from the momentum balance. However, the link between the Zuber and Findlay approach and the two-fluid model has been established in this paragraph.

The set of six equations (5), (7), (13a) and (13b) is summarized in Table 1. This set of equations is retained to calculate the six variables (R_g, R_l, R_s, U_g, U_l, U_s). This set of equations is now applied in the airlift loop reactor.

3. Global model of gas–liquid–solid airlift reactor

The airlift reactor, plotted in Fig. 1, is divided into four zones (Fig. 2). Zone 1 is the three phase co-current up-flow, located on the right side of the internal wall: it will be called the riser. Zone 2 is located above the internal wall; it constitutes a singularity at the top of the airlift reactor, downstream from the riser. Zone 3 is the three phase co-current down-flow, located on the left side of the internal wall: it will be called the downcomer. Zone 4 is located below the internal wall; it constitutes a singularity at the bottom of the airlift reactor, downstream from the downcomer. The subscripts r and d stand for, respectively, the riser and the downcomer. In the three phase co-current up-flow and down-flow regions (Zones 1 and 3), the flow is assumed to be steady state and fully developed. The first assumption on steady state flow is acceptable since no low frequency motion has been detected in the airlift. It would be different in bubble columns (Mudde and Simonin, 1999). The second assumption on fully developed flow is related to the size of the airlift: the height (more than 2.5 m) is ten times larger than the half-width (0.25 m). Thus, recirculating flow regions are limited to a small part of each zone. Of course, this is a simplification since there is

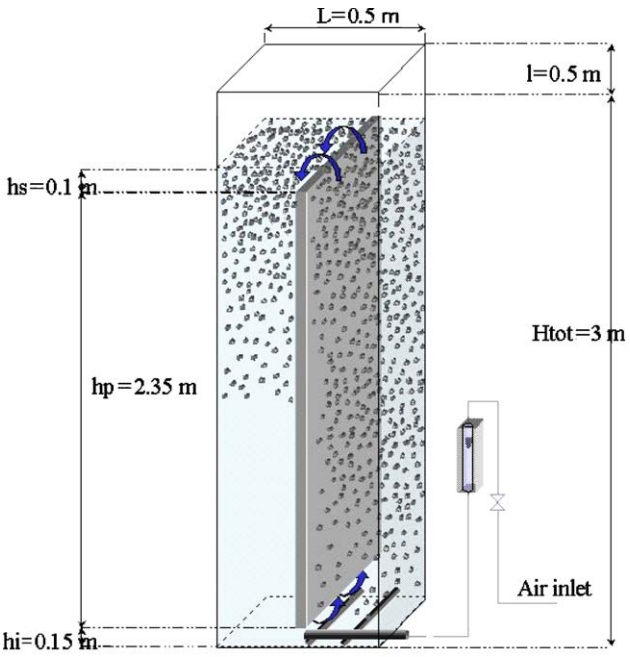

Fig. 1. Experimental pilot.

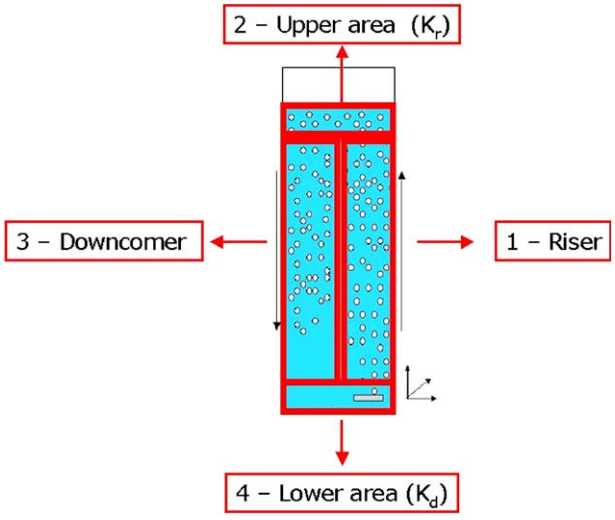

Fig. 2. Global model representation.

Table 2
GLS model in the airlift reactor

Downcomer	Riser
$R_{g,d}U_{g,d} = j_{g,d}$	$R_{g,r}U_{g,r} = j_{g,r}$
$R_{l,d}U_{l,d} = j_{l,d}$	$R_{l,r}U_{l,r} = j_{l,r}$
$R_{s,d}U_{s,d} = j_{s,d}$	$R_{g,r}U_{g,r} = j_{s,r}$
$R_{g,d} + R_{l,d} + R_{s,d} = 1$	$R_{g,r} + R_{l,r} + R_{s,r} = 1$
$U_{g,d} = C_{0,g,d}(j_{g,d} + j_{l,d} + j_{s,d}) + G_d$	$U_{g,r} = C_{0,g,r}(j_{g,r} + j_{l,r} + j_{s,r}) + G_r$
$U_{s,d} = C_{0,s,d}(j_{g,d} + j_{l,d} + j_{s,d}) + S_d$	$U_{s,r} = C_{0,s,r}(j_{g,r} + j_{l,r} + j_{s,r}) + S_r$

Global equations
Liquid momentum balance:
$(\rho_{M,d} - \rho_{M,r}) \cdot H \cdot g = \frac{1}{2}\rho_l(K_r + K_d)j_l^2$
Solid mass conservation:
$\frac{R_{s,r}+R_{s,d}}{2} = \mathrm{FR} * \varepsilon$

a developing zone above the gas injection, and in the downcomer, the upper part is aerated and there is no gas in the lower part.

3.1. GLS model in the airlift

The equations reported in Table 1 are now developed in the riser (Zone 1, subscript r) and the downcomer (Zone 3, subscript d). These 12 equations can be used to calculate the 12 unknowns: six velocities and six phase fractions. Closure relations are needed for the bubble and particle slip velocities G and S, and for the empirical constants $C_{0,k}$. Since the airlift is closed to the liquid and to the solid, the superficial velocity of liquid and of solid in the riser are equal to the superficial velocity of liquid and of solid in the downcomer. The main problem is that these two superficial velocities are unknown. The single superficial velocity which is known is related to the gas flow injected in the riser of the airlift. Thus, two additional closure relations are needed to derive the liquid and solid superficial velocities.

In terms of solid fraction, one must verify that the solid quantity is constant. In the experiments, the amount of solid introduced into the airlift is known. FR stands for the volumetric filling rate of the airlift reactor, and ε is the compacity rate ($\varepsilon = 60\%$ for particles). $\mathrm{FR} * \varepsilon$ thus corresponds to the solid volume fraction. In practice, the riser and downcomer have the same volume. The solid mass conservation must be verified as follows:

$$\frac{R_{s,r} + R_{s,d}}{2} = \mathrm{FR}\varepsilon. \tag{14a}$$

This first additional equation will enable the determination of the superficial velocity of the solid.

In order to express an additional relation to calculate the superficial velocity of the liquid, it is necessary to come back to the airlift operation. When gas is injected into the riser, the riser column is aerated. Its weight is thus smaller than the weight of the downcomer. This difference in pressure induces a liquid circulation. The liquid flow rate is then determined by a balance between the weight difference between the riser and the downcomer and the sum of all pressure drops (linear pressure drops in the riser and in the downcomer and singular pressure drops above and below the internal wall).

The linear pressure drops can be calculated in the riser and in the downcomer, using Eq. (10). The two zones 2 and 4 are characterized by singular pressure drop coefficients, denoted by K_r for the top and K_d for the bottom of the airlift; the singular pressure drops can then be derived. A loop on the pressure drop leads to the following simplified equation:

$$(\rho_{M,d} - \rho_{M,r}) \cdot H \cdot g = \tfrac{1}{2}\rho_l(K_r + K_d)j_l^2. \tag{14b}$$

This equation expresses that the difference in column weight between the riser and the downcomer is balanced by the pressure drops (the linear pressure drops being negligible compared to singular ones).

The set of 14 equations is summarized in Table 2. It enables the six phase fractions to be calculated (for each one of the three phases in the riser and in the downcomer), and also the six velocities, the solid and liquid superficial velocities, given the superficial velocity of the gas injected into the airlift reactor.

For the gas flow, different situations must be considered. Indeed, with increasing superficial gas velocity, two flow regimes can be identified whether the downcomer is aerated or not:

- Firstly, if the downward liquid velocity in the downcomer is smaller than the upward bubble slip velocity, the bubbles are not dragged into the downcomer, $R_{g,d}$ is thus considered equal to 0.
- As soon as the downward liquid velocity in the downcomer becomes larger than the upward bubble slip velocity, the bubbles are dragged into the downcomer, $R_{g,d}$ is therefore greater than 0. Moreover, according to experimental observations, the bubbles seem to be motionless in the downcomer, so that $U_{g,d}$ is assumed to be equal to 0.

Table 3
Simplified GLS airlift model

Non-aerated downcomer	Aerated downcomer
$R_{g,r} = \frac{j_g}{C_{0,g,r}(j_g+j_l+j_s)+G_r}$	Same equations
$R_{s,r} = \frac{j_{s,r}}{C_{0,g,r}(j_g+j_l+j_s)+S_r}$	
$R_{s,d} = \frac{j_s}{C_{0,g,r}(j_l+j_s)-S_d}$	+
$(\rho_{M,d} - \rho_{M,r}) \cdot H \cdot g = \frac{1}{2}\rho_l(K_r + K_d)j_l^2$	$j_s + j_l = \frac{G_d}{C_{0,g,d}}$
$\frac{R_{s,r}+R_{s,d}}{2} = \mathrm{FR} * \varepsilon$	
Five equations for five unknown variables	Six equations for six unknown variables
$R_{g,r}$, $R_{s,r}$, $R_{s,d}$, j_l, j_s	$R_{g,r}$, $R_{g,d}$, $R_{s,r}$, $R_{s,d}$, j_l, j_s

Thus, as long as the downcomer is not aerated,

$$j_{g,r} = j_g \quad \text{and} \quad j_{g,d} = 0 \quad \text{since } R_{g,d} = 0.$$

As soon as the downcomer is aerated,

$$j_{g,r} = j_g \quad \text{and} \quad j_{g,d} = 0 \quad \text{since } U_{g,d} = 0.$$

Hence, the equations from Table 2 can be simplified according to the former assumption. Table 3 sums up the equations applied to solve the gas–liquid–solid flow in the airlift loop reactor. The equations reported in Table 3 contain the following closure terms which will be explained in the next part: the bubble slip velocities: G_r and G_d, the solid slip velocities: S_r and S_d, the drift flux coefficients: $C_{0,g,r}$, $C_{0,g,d}$ and $C_{0,s,r}$, $C_{0,s,d}$ and the global singular pressure drop coefficient: $K = K_r + K_d$.

3.2. Closure relations of the GLS model in the airlift

The closure terms are discussed below: firstly, the dispersed phase slip velocities (Section 3.2.1), then the drift-flux coefficients (Section 3.2.2) and finally the pressure drop coefficients (Section 3.2.3). The two last coefficients result from CFD simulations.

3.2.1. Dispersed phase slip velocities

As aforementioned, the slip velocities of the bubble and solid particles in the riser and in the downcomer are deduced from momentum balance:

- For the bubble slip velocity:

$$G_{r,d} = \sqrt{\frac{4}{3} g \frac{d_g}{C_{D,g}} \frac{(\rho_{M,r,d} - \rho_g)(1 - R_g)}{\rho_{M,r,d} - \rho_g R_g}}. \tag{15a}$$

The drag coefficient $C_{D,g}$ is given by Karamanev and Nikolov (1992) for an ellipsoidal bubble: $C_{D,g} = 0.95$. This drag coefficient which has been previously used by Cockx et al. (1997) and Couvert (2000) is suitable for characterizing bubble drag force in this airlift loop reactor.

- For the solid slip velocity:

$$S_{r,d} = \sqrt{\frac{4}{3} g \frac{d_s}{C_{D,s}} \frac{|\rho_{M,r,d} - \rho_s|(1 - R_s)}{\rho_{M,r,d} - \rho_s R_s}} \times \frac{\rho_{M,r,d} - \rho_s}{|\rho_{M,r,d} - \rho_s|}. \tag{15b}$$

This relation is developed in the knowledge that the solid density ρ_s can be smaller than the mixture (water–air) density, implying that the solid slip velocity may be negative. The solid drag coefficient is defined below by the classical correlation concerning rigid spherical particles.

$$C_{D,s} = \frac{24}{Re_p}(1 + 0.15 Re_p^{0.687})(1 - R_s)^{-1.7}.$$

With the particle Reynolds number defined as

$$Re_p = \frac{\rho_l d_s |S|}{\mu_l}.$$

One can thus calculate the liquid and solid slip velocities for each superficial gas velocity.

3.2.2. Drift-flux coefficients

The drift-flux coefficient is defined in two-phase bubbly flow as follows:

$$C_{0,g} = \frac{\langle \alpha_g j_M \rangle}{\langle \alpha_g \rangle \langle j_M \rangle} \tag{16}$$

with $j_M = \alpha_g v_g + \alpha_l v_l$.

If the spatial distributions of phase fraction and gas–liquid mixture velocity are available, the drift flux coefficient can be determined. In fact, the drift-flux coefficient concerning the gas phase ($C_{0,g}$) was calculated from CFD results (Talvy, 2003) in gas–liquid flow in the same airlift reactor. These coefficients are assumed to be the same for a gas–liquid–solid flow, for a given superficial gas velocity. CFD simulations in three phase flow show that the solid is uniformly distributed in the cross-section of the airlift. The gas is not uniformly distributed. Indeed, the density of the particles is much closer

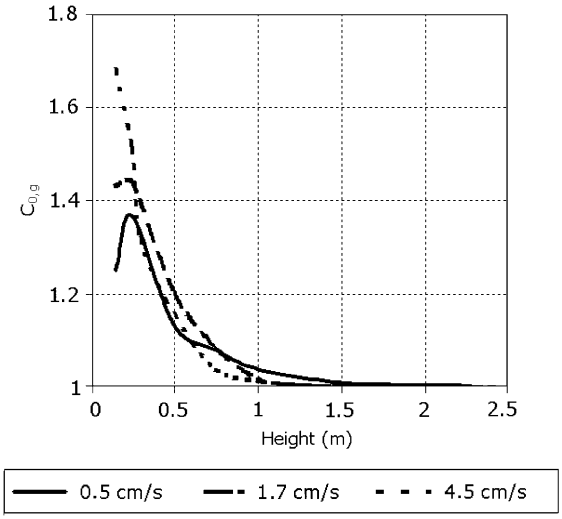

Fig. 3. Drift-flux coefficient in the riser.

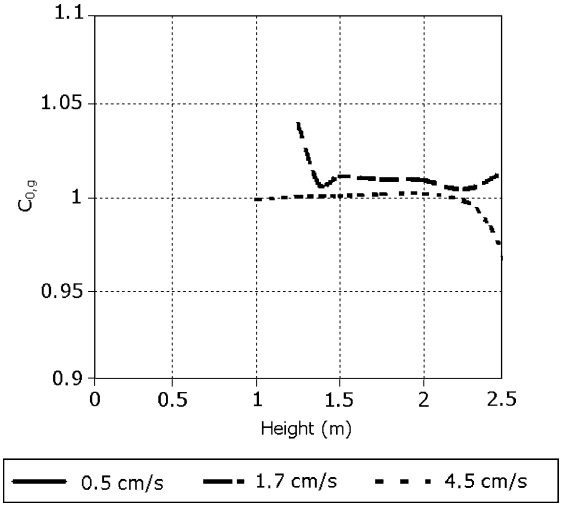

Fig. 4. Drift-flux coefficient in the downcomer.

to the liquid density than the gas. Thus, the solid particles follow the liquid motion, and the dispersion of the gas by the turbulence of the liquid can be assumed to be weakly affected by the solid particles. The analysis of the model's sensitivity to this coefficient will be discussed later in this paper.

Fig. 3 presents the variation of the CFD simulated drift flux coefficient $C_{0,g}$ in the riser and Fig. 4 in the downcomer. According to Fig. 3, in the riser, the highest values of $C_{0,g}$ are located near the region of the aerator. Indeed, in this region, the flow is not uniform so that the bubbles are not uniformly distributed in the cross section, as they escape from the sparger. Moreover the higher the superficial gas velocity, the higher is the value of $C_{0,g}$ in this region. The axial evolution of the drift flux coefficient $C_{0,g}$ in the riser can be related to the axial evolution of the gas fraction, the axial gradient of the gas fraction being large above the injection and almost

Table 4
Pressure coefficient values from CFD

Superficial gas velocity	0.5 cm/s	1.7 cm/s	4.5 cm/s
K	15	15	11

constant downstream. In the present approach, limited to fully developed flow, the volume average value of $C_{0,g}$ is close to 1.1 in the riser and 1 in the downcomer. These values are in agreement with the values obtained by Vial et al. (2002) for bubbles rising in a global homogeneous regime.

The drift-flux coefficient for the solid phase is fixed at unity, after CFD simulations showed that the solid phase is uniformly distributed in the cross section of the riser as well as in the cross section of the downcomer (Talvy, 2003).

3.2.3. Pressure drop coefficient

The singular pressure drops above and below the internal wall were calculated from CFD simulations in gas–liquid flow in the airlift (Talvy, 2003). The singular pressure drop coefficients are defined as follows:

$$\Delta P_r = \tfrac{1}{2}\rho_l K_r j_l^2, \tag{17a}$$

$$\Delta P_d = \tfrac{1}{2}\rho_l K_d j_l^2, \tag{17a}$$

where ΔP_r represents the singular pressure drop above the internal wall (at a height of 2.15 m from the bottom), downstream from the riser and the downcomer and ΔP_d represents the singular pressure drop below the internal wall (at 0.3 m from the bottom). The two-phase flow CFD simulations thus provide the global singular pressure drop coefficient value of $K = K_d + K_r$.

Table 4 provides the values of this coefficient for three different superficial gas velocities. The coefficient K seems to be constant, at least for the smaller gas velocities. In the global model, K will thus be firstly fixed at 15; afterwards analysis of the model's sensitivity to this parameter will be discussed.

4. Experimental setup

All the data related to a gas–liquid–solid airlift reactor, used in this paper, were carried out by Couvert (2000). Detailed informations are given in Couvert et al. (1999, 2004).

4.1. Laboratory pilot

The reactor is a parallelepiped vessel of 3 m in height and 0.5 m in width and depth. It is equipped with a baffle in its middle as described in Fig. 1. The baffle position is fixed. The reactor was initially filled up with tap water up to 2.6 m height. The global circulation of both liquid and solid particles is induced by air injection, which is ensured by two horizontal cylindrical membrane spargers (Flexazur

Table 5
Physical values concerning the different phases

Parameters	Values	Units
ρ_g	1.2	kg/m^3
ρ_l	998	kg/m^3
ρ_s	934	kg/m^3
d_s	3.76	mm
ε	60	%
H	2.35	m

Table 6
Bubble characteristics according to superficial velocity

Superficial velocity	0.5 cm/s	1.7 cm/s	4.5 cm/s
Bubble diameter	2.7 mm	3.4 mm	4.3 mm

T415 membrane covering Plexiglas cylinders), located at the bottom-right of the reactor. The outside diameter of each cylindrical membrane sparger is 40 mm. The injectors being made from a perforated membrane, the bubble diameters are calibrated by the superficial gas velocity as shown by Couvert (2000), who measured the bubble diameters for different superficial gas velocities. The liquid height below the internal wall is 150 mm and the axis of the cylindrical membrane spargers is located at 100 mm above the bottom of the pilot.

4.2. Method

Holes distributed along the height of the reactor walls assure the pressure measurement, in order to deduce volume gas fraction. The overall gas hold-up in the airlift is determined by using a volume expansion technique and is measured from the difference between the ungassed and gassed liquid level. Solid phase is composed of plastic particles whose properties are noted in Table 5. In the experiments, two solid volumetric filling rates (FR) were studied: 20% and 40%. The solid hold-up was measured thanks to a trapping box, sampling a certain amount of liquid and particles in the flow. Liquid velocity is determined by salt tracing technique whose concentration is tracked by a conductimeter probe. This device also allows the measurement of mixing parameters from which the liquid velocity is deduced. 100 g of NaCl were injected at the top of the downcomer. A Tacussel Xe 100 probe was immersed 500 mm below the free surface of the downcomer. The probe is related to a Tacussel CD 6N conductimeter. The range of applied superficial velocity goes from 0 to 4.54 cm/s, in order to remain close to homogeneous flow.

4.3. Physical properties

Table 5 describes the main physical properties of the system.

Table 6 presents the bubble characteristics according to superficial velocity

5. Global model results and discussion

Experimental and modelled values are compared in terms of gas and solid volume fractions. Two volumetric FR are chosen: FR = 20% and 40%. Gas volume fraction, particle slip velocity and sensitivity to drift-flux coefficient are discussed.

5.1. Results with FR = 20%

The airlift reactor is studied for different superficial gas velocities (0–4.54 cm/s). The global gas volume fraction as well as the solid volume fraction in the riser and the downcomer are first discussed.

The global gas fraction is defined as follows:

$$R_g = \frac{R_{g,r} + R_{g,d}}{2}.$$

This global gas fraction in the airlift is plotted versus the superficial gas velocity in Fig. 5. The gas–liquid–solid airlift model is compared to experiments in gas–liquid–solid and gas–liquid experiments. As noticed by Couvert (2000), with such an amount of solid particles (FR = 20%), the global gas hold-up is not affected by the presence of the particles in the airlift loop reactor: for a given superficial gas velocity, the global gas fraction in the airlift in three phase flow is close to its value in two phase flow. The model developed in the former paragraphs is shown to be in very good agreement with the experimental data in terms of global gas volume fraction. The result confirms that neglecting the interaction between bubbles and particles is relevant.

However, the gas volume fraction in the airlift operating at high gas superficial velocity is smaller in three-phase than

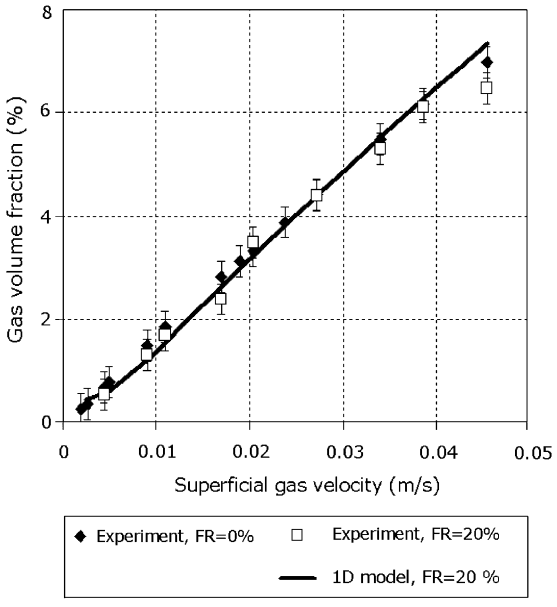

Fig. 5. Global gas volume fraction (FR = 20%).

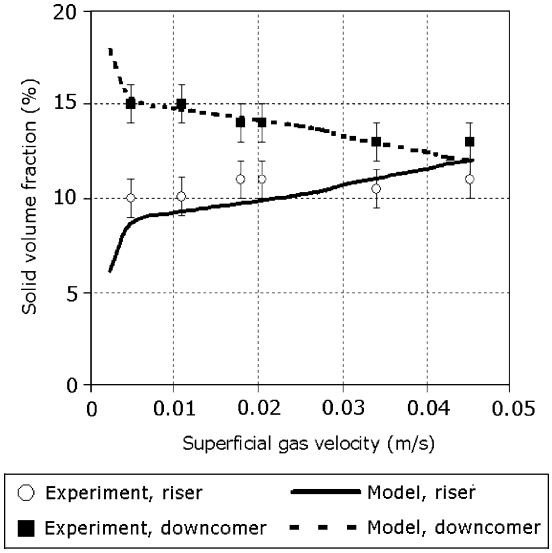

Fig. 6. Global solid volume fraction (FR = 20%).

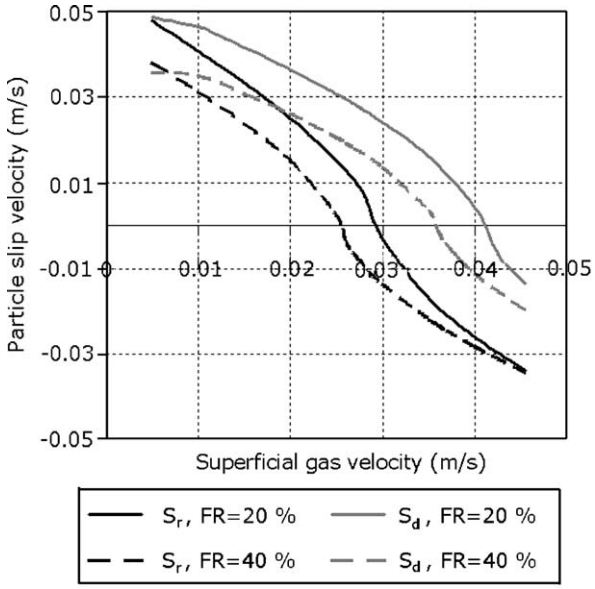

Fig. 7. Particle slip velocity.

in two-phase flow, indicating that at high gas superficial velocity, the particles interfere with the bubble trajectory so that the rate of bubble coalescence increases.

The solid volume fraction is plotted versus the superficial gas velocity, in the riser and in the downcomer in Fig. 6. The model results are in good agreement with experimental data. Three zones can be identified in Fig. 6. Firstly, for a superficial gas velocity less than 0.5 cm/s, the model predicts that a great amount of particles will be dragged into the downcomer (more than 15%). As the downcomer is not yet aerated and as particle density is less than that of water, many more particles have to be dragged into the downcomer in order to satisfy the global momentum balance within the reactor. Freitas et al. in their global modelling considered a homogeneous distribution of the solid particles in the airlift whatever the superficial gas velocity, by developing a "pseudo-homogeneous mixture phase". This assumption is thus not valid here for low superficial gas velocities.

For superficial gas velocities between 0.5 and 4.5 cm/s, the solid hold-up tends to balance itself between the riser and the downcomer, the mixture density of the mixture (ρ_M) becoming smaller while the gas superficial velocity and the associated gas hold-up are increasing. Around the superficial gas velocity of 3 cm/s, the particle slip velocity in the riser (S_r) (Fig. 7) becomes negative, corresponding to the fact that mixture density (ρ_M) is lower than the particle density ρ_s in the riser according to Eq. (15b). At this point, neither gas nor solid volume fraction is affected by this sign switching. Besides, around superficial gas velocities of 4.25 cm/s, the gas volume fraction in the downcomer implies that ρ_M is less than ρ_s, owing to the fact that particle slip velocity in the downcomer (S_d) is becoming negative (Fig. 7). Experimentally, one can expect that, at high gas velocity, solid volume fraction is equally distributed between the riser and the downcomer. It can also be supposed that particles can be considered as an obstacle to the motion of the bubbles which would coalesce and then decrease the total gas volume fraction. For that reason, the mixture density should remain higher than or equal to the solid density so that $R_{s,r}$ would always be slightly higher than or equal to $R_{s,d}$. However, this hypothesis needs more experimental data to be confirmed.

As far as the sensitivity to K value is concerned, it is found that the only variable really affected by a variation in the singular pressure drop coefficient is the global gas volume fraction. Its value varies no more than 5%. Thus, the choice of a single value of K and also the need of a single CFD simulation to provide it, is confirmed.

A relation between $R_{g,d}$ and $R_{g,r}$, coming from the different equations applied in the model, can be proposed. The relation found between these two variables is in agreement with the relation established by Heijnen et al. (1997).

$$(R_{g,r} - R_{g,d}) - \left(\frac{\rho_l - \rho_s}{\rho_l}\right)(R_{s,d} - R_{s,r}) = \left[\frac{1}{2} K \frac{j_l^2}{gH}\right]. \quad (18)$$

According to Eq. (18), equivalent to Eq. (14b), the second term in the left hand side of the equation will always be positive, whatever the value of the particle density compared to water density. If ρ_s is higher than ρ_l, then $R_{s,r}$ would be higher than $R_{s,d}$, or if ρ_s is lower than ρ_l, then $R_{s,r}$ would be lower than $R_{s,d}$. This implies that the presence of the particles will always diminish the liquid velocity compared to a case without solid particles (Heijnen et al., 1997). Fig. 8 represents the liquid velocity for different solid particle loading values. Increasing solid hold-up involves a decrease in liquid velocity. Indeed, the higher the solid volume

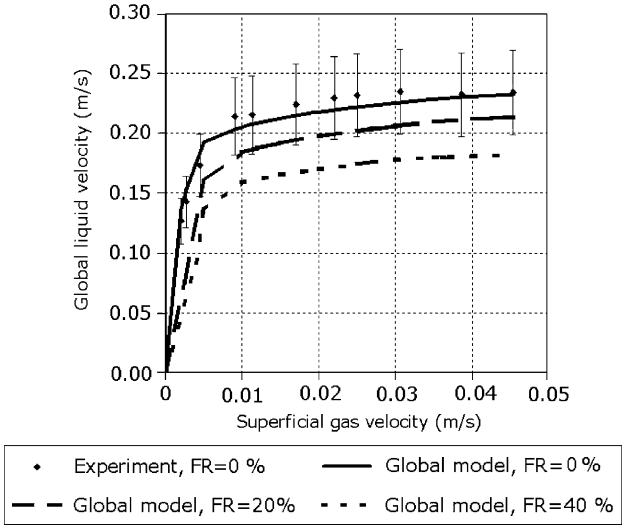

Fig. 8. Global liquid velocity.

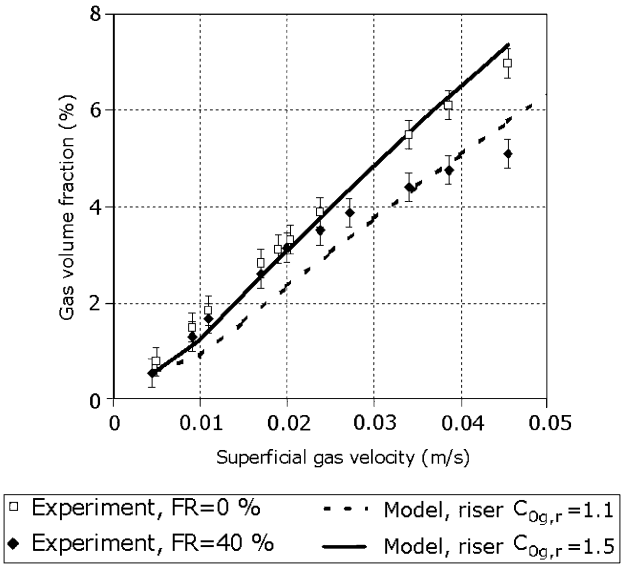

Fig. 9. Global gas volume fraction (FR = 40%).

fraction in the reactor, the more energy will be necessary to put particles in motion. This energy is extracted from liquid motion as written in equation in Table 3 where the sum of j_s and j_l is equal to the bubble slip velocity in the downcomer which depends only on physical properties of the different phases and bubble drag coefficient.

To conclude at this point, the global model is able to predict the gas and solid volume fractions in the riser and in the downcomer. Thanks to this validation, more information can be extracted, especially on the behaviour of the particles in the reactor. At low gas velocity, the particles gather together in the downcomer but with increasing gas flow rates the particles are distributed more evenly in the reactor. Their slip velocity represents an important parameter concerning the different regimes occurring in the airlift. Although there is good agreement between experiments and the model, the latter remains limited as soon as the flow causes coalescence phenomena.

5.2. Results with FR = 40%

At a higher filling rate of particles in the airlift reactor (40%) the same model was applied. Experimentally, it can be noticed from Fig. 9 that the gas hold-up with such a solid loading rapidly differs from the gas hold-up without solid particles. For a superficial gas velocity below 2.5 cm/s, the gas volume fraction in the presence of particles is similar to the two-phase flow case (Fig. 9). For a superficial gas velocity higher than 2.5 cm/s, the particles, at this filling rate, may interfere with the bubbles making the latter coalesce. The larger bubbles formed could escape faster and thus induce a lower global gas volume fraction.

For a superficial gas velocity less than 2 cm/s, the current model ($C_{0,g,r} = 1.1$) is valid, since the particles do not seem to interfere with the bubbles. However, for a higher superficial gas velocity, the model overestimates the global gas fraction. Indeed, coalescence phenomena should be taken into consideration.

Nevertheless, thanks to the Zuber and Findlay model, it is possible to lump this phenomenon in the drift-flux coefficient ($C_{0,g,r}$). Indeed, the increase in the value of $C_{0,g,r}$ involves an increase in bubble velocity and thus a decrease in gas hold-up. A characteristic value of $C_{0,g,r}$ for such a heterogeneous flow can be taken as 1.5. This value is in the same range of the values obtained by Vial et al. (2000) for a heterogeneous bubbly flow. Therefore, the closure value of this parameter has been modified in the model. With this value, the model is able to predict the global gas hold-up for a superficial velocity between 2.5 cm/s and 4 cm/s as shown in Fig. 9.

This observation is also in agreement with the results of Freitas et al. who worked with a IL-ALR as well. Even though their particle and airlift dimensions are different, the same trend concerning the increase of the drift flux coefficient C_0 with gas flow rate can be noticed. Freitas et al. increased this coefficient from 1.13 to 2.21.

The solid volume fraction in the riser and in the downcomer is plotted in Fig. 10. The solid volume fraction is compared for two values of the coefficient $C_{0,g,r}$. For $C_{0,g,r}$ of 1.1, like the global gas volume fraction, the solid hold-up is well represented by the model for a superficial gas velocity less than 2.5 cm/s. Above this gas velocity, the model values move away from the experimental data and solid fraction inversion occurs for a superficial gas velocity equal to about 4 cm/s. If the coefficient $C_{0,g,r}$ is increased to 1.5, the model is able to account for the experimental results. According to Fig. 7, as soon as the particle slip velocity becomes negative in the riser (around 2.5 cm/s), bubble coalescence occurs. Indeed, Fig. 7 shows that the particle slip velocity becomes negative for a superficial gas velocity of

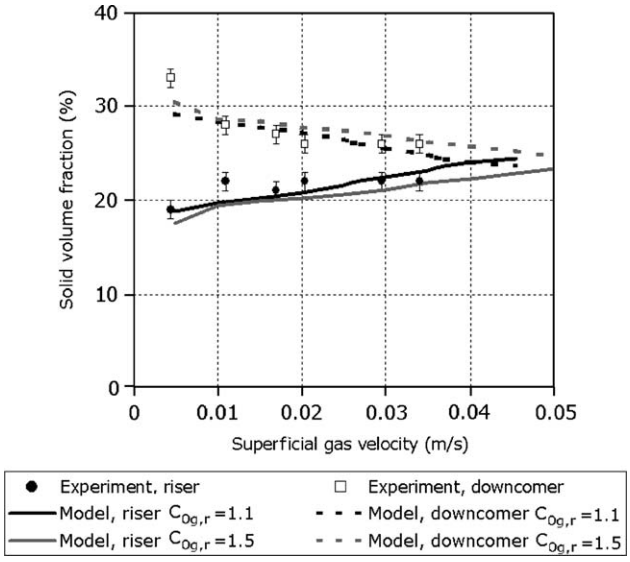

Fig. 10. Global solid volume fraction (FR = 40%).

approximately 2.5 cm/s, which corresponds to the superficial gas velocity from which the global gas-hold-up for FR of 40% particles (FR = 0%).

6. Conclusion

The study of an internal airlift loop reactor was carried out with a three phase gas–liquid–solid system. The particles used in the experimental setup are lighter than water and have a diameter close to the bubble diameter. The effect of the solid loading on the hydrodynamics is taken into account for two solid hold-up values (20% and 40%). The experimental results were obtained by Couvert (2000). To characterize the system, a global model approach was developed. In order to close the system, CFD simulations were run to provide the drift flux coefficients ($C_{0,g}$ and $C_{0,s}$) and the pressure drop coefficient (K).

For the first filling rate of particles (20%), it was noticed that the presence of the particles, in the range of superficial gas velocities studied, did not interfere much with the bubbles, so that the global gas volume fraction in three phase flow is nearly identical to the two phase flow gas volume fraction. The model predictions concerning the solid volume fraction in the riser and in the downcomer are in good agreement with the experimental data. At this point, it was considered that single CFD simulation was sufficient to reach a correct value of the pressure drop and drift flux coefficient.

For a higher solid filling rate (40%), at low superficial gas velocity, the global model correctly predicts gas and solid volume fractions. However, at higher superficial gas velocity, the global model has to be improved to take into account bubble coalescence. Modifying the gas drift-flux coefficient in the riser enhances the results concerning the global gas volume fraction and the particle distribution in the reactor.

In conclusion, this paper presents a simplified global model, in agreement with experimental results, with physical closure terms, several of them coming from a restricted number of CFD simulations. In particular, CFD simulations were run to provide the drift flux coefficients ($C_{0,g}$ and $C_{0,s}$). The availability of drift flux coefficients is mainly related to the local modelling of the drift velocity in the numerical simulations. This local drift velocity enables to simulate correctly the dispersion of gas bubbles by the turbulence. The global drift velocity, as well as the global drift coefficient, is closely related to the non-uniformity of the gas dispersion in the airlift. The analytical modelling of the drift flux coefficients, based on local modelling of drift velocity and gas dispersion constitutes a perspective of this work. The drift modelling constitutes the key point to reconcile 1D two-fluid model to drift flux model of Zuber and Findlay (1965). Another issue of this work is to develop a axial model of the three-phase flow hydrodynamics, in which the drift flux coefficient ($C_{0,g} - 1$) could be related to the axial gradient of gas fraction, in terms of global dispersion coefficient D_{global}.

Notation

a	projected interfacial area, m^2
A	cross sectional area, m^2
C_0	drift flux coefficient, (dimensionless)
C_D	drag coefficient, (dimensionless)
d	dispersed phase diameter, m
D	diffusivity (dispersion coefficient), $m^2\,s^{-1}$
g	gravity, $m\,s^{-2}$
G	bubble slip velocity, $m\,s^{-1}$
j	superficial velocity, $m\,s^{-1}$
K	pressure drop coefficient
L	wall transfer
M_l	interphase momentum exchange, $kg\,m^{-1}\,s^{-2}$
P	pressure, Pa
Q	mass flow rate, $kg\,s^{-1}$
R	volume fraction, (dimensionless)
Re	Reynolds number, (dimensionless)
s	surface element, m^2
S	solid slip velocity, $m\,s^{-1}$
u	local velocity, $m\,s^{-1}$
U	average velocity, $m\,s^{-1}$
v	velocity, $m\,s^{-1}$
V	volume, m^3

Greek letters

α	local volume fraction
ε	solid compacity
ρ	density, kg/m^3
τ	shear stress, $kg\,m^{-1}\,s^{-2}$

Superscripts

i	interfacial
w	wall

Subscripts

d	downcomer
dr	drift
g	gas
k, l	referring to a phase
l	liquid
r	riser
s	solid

References

Cockx, A., 1998. Modélisation de contacteurs gaz-liquide: application de la mécanique des fluides numérique aux airlifts. Thèse de Doctorat de l'Institut National des Sciences Appliquées de Toulouse.

Cockx, A., Liné, A., Roustan, M., Do-Quang, Z., Lazarova, V., 1997. Numerical simulation and physical modeling of hydrodynamics of an airlift internal loop reactor. Chemical Engineering Science 52, 3793–3797.

Couvert, A., 2000. Etude d'un réacteur airlift rectangulaire à recirculation interne. Ph.D. Thesis, INSA, Toulouse.

Couvert, A., Roustan, M., Chatellier, P., 1999. Two-phase hydrodynamic study of a rectangular airlift loop reactor with an internal baffle. Chemical Engineering Science 54 (21), 5245–5252.

Couvert, A., Bastoul, D., Roustan, M., Chatellier, P., 2004. Hydrodynamic and mass transfer study in a rectangular three phase airlift loop reactor. Chemical Engineering and Processing 43 (11), 1381–1387.

Freitas, C., Fialova, M., Zahradnik, J., Teixera, J.A., 1999. Hydrodynamic model for three-phase internal and external loop airlift reactor. Chemical Engineering Science 54, 5253–5258.

Heijnen, J.J., van Loodsdrecht, M.C.M., Mulder, A., Tijhuis, L., 1992. Formation of biofilms in a biofilm air-lift suspension reactor. Water Science and Technology 26 (3–4), 647–654.

Heijnen, J.J., Hols, J., van der Lans, R.G.M.M., van Leeuwen, H.L.J.M., Mulder, A., Welteverde, R., 1997. A simple hydrodynamic model for liquid circulation velocity in a full scale two- and three-phase internal airlift reactor operating in the gas recirculation regime. Chemical Engineering Science 52, 2527–2540.

Karamanev, D.G., Nikolov, L.N., 1992. Free rising sphere do not obey Newton's law for free settling. A.I.Ch.E. Journal 38 (11), 1873–1846.

Merchuk, J.C., 2003. Airlift bioreactors: review of recent advances. The Canadian Journal of Chemical Engineering 81 (3–4), 324–337.

Mudde, R.F., Simonin, O., 1999. Two and three-dimensional simulations of a bubble plume using two-fluid model. Chemical Engineering Sciences 54 (21), 5061–5069.

Nicollela, C., van Loodrecht, M.C.M., Heijnen, J.J., 1999. Identification of mass transfer parameters in three-phase biofilm reactors. Chemical Engineering Science 54, 3143–3152.

Oey, R.S., Mudde, R.F., Portela, L.M., van den Akker, H.E.A., 2001. Simulation of a slurry airlift using a two-fluid model. Chemical Engineering Science 56, 673–681.

Saez, A.E., Marquez, M.A., Roberts, G.W., Carbonell, R.G., 1998. Hydrodynamic model for gas-lift reactors. A.I.Ch.E. Journal 44, 1413–1423.

Siegel, M.H., Robinson, C.W., 1992. Applications of airlift gas–liquid–solid reactors in biotechnology. Chemical Engineering Science 47 (13/14), 3215–3229.

Simonin, O., Viollet, P.L., 1990. Modelling of turbulent two-phase jets loaded with discrete particles. In: Hewitt, G., Mayinger, F., Riznic, J.R. (Eds.), Phase Interface Phenomena in Multiphase Flow. Hemisphere Publ. Corp., Washington, DC, pp. 259–270.

Talvy, S., 2003. Airlift et colonne à bulles en écoulements gaz-liquide et gaz-liquide-solide. Ph.D. Thesis, INSA, Toulouse.

van Benthum, W.A.J., van der Lans, R.G.J.M., van Loosdrecht, M.C.M., Heijnen, J.J., 2000. The biofilm airlift suspension extension reactor—II: three phase hydrodynamics. Chemical Engineering Science 55, 699–711.

Vial, C., Poncin, S., Wild, G., Midoux, M., 2000. Experimental and theoretical analysis of hydrodynamics in the riser of an external loop reactor. Chemical Engineering Science 57, 4745–4762.

Vial, C., Lalaoui, N., Poncin, S., Midoux, M., Wild, G., 2002. Régimes d'écoulement dans les écoulements à gazosiphon à recirculation externe, 4èmes journées francophone sur les réacteurs gaz-liquide et gaz-liquide-solide.

Zuber, N., Findlay, J.A., 1965. Average volumetric concentration in two-phase flow systems. International Journal of Heat Mass Transfer 87, 453–468.